Stochastic kinetics of ribosomes: Single motor properties and collective behavior

Ashok Garai,[1] Debanjan Chowdhury,[1] Debashish Chowdhury,[1,*] and T. V. Ramakrishnan[2,3]
[1]*Department of Physics, Indian Institute of Technology, Kanpur 208016, India*
[2]*Department of Physics, Banaras Hindu University, Varanasi 221005, India*
[3]*Department of Physics, Indian Institute of Science, Bangalore 560012, India*
(Received 30 March 2009; revised manuscript received 4 June 2009; published 9 July 2009)

Syntheses of protein molecules in a cell are carried out by ribosomes. A ribosome can be regarded as a molecular motor which utilizes the input chemical energy to move on a messenger RNA (mRNA) track that also serves as a template for the polymerization of the corresponding protein. The forward movement, however, is characterized by an alternating sequence of translocation and pause. Using a quantitative model, which captures the mechanochemical cycle of an individual ribosome, we derive an *exact* analytical expression for the distribution of its dwell times at the successive positions on the mRNA track. Inverse of the average dwell time satisfies a "Michaelis-Menten-type" equation and is consistent with the general formula for the average velocity of a molecular motor with an unbranched mechanochemical cycle. Extending this formula appropriately, we also derive the exact force-velocity relation for a ribosome. Often many ribosomes simultaneously move on the same mRNA track, while each synthesizes a copy of the same protein. We extend the model of a single ribosome by incorporating steric exclusion of different individuals on the same track. We draw the phase diagram of this model of ribosome traffic in three-dimensional spaces spanned by experimentally controllable parameters. We suggest new experimental tests of our theoretical predictions.

DOI: 10.1103/PhysRevE.80.011908 PACS number(s): 87.16.ad

I. INTRODUCTION

Ribosome is one of the largest and most complex intracellular cyclic molecular machines [1–4] and it plays a crucial role in gene expression [5]. It synthesizes a protein molecule, which is a heteropolymer of amino-acid subunits, using a messenger RNA (mRNA) as the corresponding template; this process is called *translation* (of the genetic message). Monomeric subunits of RNA are nucleotides and triplets of nucleotides constitute a codon. The dictionary of translation relates each type of possible codon with one species of amino acid. Thus, the sequence of amino acids on a protein is dictated by the sequence of codons on the corresponding template mRNA. The polymerization of protein takes places in three stages which are identified as *initiation*, *elongation* (of the protein), and *termination*. In this paper, we focus almost exclusively on the elongation stage.

A ribosome is often treated as a molecular motor for which the mRNA template also serves as a track. In each step, it moves forward on its track by one codon by consuming chemical fuel [e.g., two guanosine triphosphate (GTP) molecules]. Simultaneously, in each step, it also elongates the protein by adding an amino acid; the correct sequence of the amino acids required for polymerizing a protein is dictated by the codon sequence on the mRNA template. Therefore, it may be more appropriate to regard a ribosome as a mobile workshop that provides a platform for operation of several tools in a well-coordinated manner. Our main aim is to predict the effects of the mechanochemical cycle of individual ribosomes, in the elongation stage, on their experimentally measurable physical properties. We first focus on the single-ribosome properties which characterize their stochastic movement on the track in the absence of interribosome interactions. Then we consider the additional effects of the steric interactions of the ribosomes and those of the rates of initiation and termination of translation on the collective spatiotemporal organization of the ribosomes on a track.

The stochastic forward movement of a ribosome is characterized by an alternating sequence of pause and translocation. The sum of the durations of a pause and the following translocation defines the time of a dwell at the corresponding codon. Recently, using an ingenious method, the distribution $f(t)$ of the dwell times of a ribosome has been measured [6]. We present a systematic derivation of this distribution from a detailed kinetic theory of translation which incorporates the mechanochemical cycle of individual ribosomes.

The *exact* analytical expression for $f(t)$ which we derive here is, in general, a superposition of several exponentials. On the other hand, it has been claimed [6] that the difference of two exponentials fits the experimentally measured $f(t)$ very well. We reconcile these two observations by identifying the parameter regime where our theoretically derived $f(t)$ is, indeed, well approximated by difference of two exponentials [7–11]. Moreover, we show that $\langle t\rangle^{-1}$, inverse of the mean-dwell time, satisfies a *Michaelis-Menten-like equation* [12]. The reason for this feature of the mean-dwell time is traced to the close formal similarity between the mechanochemical cycle of a ribosome and the catalytic cycle in the Michaelis-Menten theory of enzymes [12].

The elongation of the growing protein by one amino acid is coupled to the translocation of the ribosome by one codon. Therefore, $\langle t\rangle^{-1}$ is also the average velocity $\langle V\rangle$ of a ribosome on the mRNA track. An analytical expression for the average velocity of a molecular motor, whose mechanochemical cycle is unbranched, was derived by Fisher and Kolomeisky [13] in the context of motors involved in intracellular transport of cargoes [14]. The mechanochemical

*Corresponding author; debch@iitk.ac.in

cycle of the ribosome in our model is, at least formally, a special case of the cycle in the Fisher-Kolomeisky model. In this special case, the Fisher-Kolomeisky formula for the average velocity of the molecular motor, indeed, reduces to the expression for $\langle t\rangle^{-1}$ in our model of ribosome.

The average velocity of a ribosome can be reduced also by applying an external force (called a load force) that opposes the natural movement of the ribosome on its track. The force-velocity relation $\langle V\rangle(F)$ (i.e., the variation of the average velocity $\langle V\rangle$ of a motor with increasing load force F) is one of the most important characteristics of a molecular motor. Inspired by the recent progress in the single-ribosome imaging and manipulation techniques [6,15–21], we extend the formula for $\langle t\rangle^{-1}$ appropriately to derive $\langle V\rangle(F)$ for single ribosomes. The smallest load force which is just adequate to stall a molecular motor on its track is called the stall force F_s. We also predict the dependence of F_s on the availability of the amino-acid monomers and the concentration of GTP molecules.

Our theoretical predictions for $f(t)$, $\langle V\rangle(F)$, and F_s show explicitly how these quantities depend on various experimentally controllable parameters. Deep understanding of these dependences will also help in controlling various features of $f(t)$, $\langle V\rangle(F)$, and F_s. In principle, the validity and accuracy of our theoretical predictions can be tested by repeating *in vitro* experiments of Ref. [6] for several different concentrations of the amino-acid monomers and GTP molecules.

Often many ribosomes simultaneously move on the same mRNA track, while each synthesizes separately a copy of the same protein. We refer to such collective movement of ribosomes on a mRNA strand as ribosome traffic because of its superficial similarity with vehicular traffic [22]. In most of the earlier theoretical studies of ribosome traffic, individual ribosomes have been modeled as hard rods and their steric interactions have been captured by mutual exclusion [23–32]. Thus, all those models may be regarded as totally asymmetric simple exclusion process (TASEP) for hard rods [33,34]. In some recent works [35,36], we have extended these TASEP-type models of ribosome traffic by capturing the essential steps of the mechanochemical cycle of individual ribosomes. We have also reported the variation of the average rate of protein synthesis with increasing population density of the ribosomes on the track. In this work, we present the phase diagrams of the model of ribosome traffic.

In the earlier TASEP-type models of ribosome traffic [23–32], the phase diagrams were plotted in a two-dimensional plane spanned by α and β, which determine the rates of initiation and termination. In this paper, we plot the three-dimensional phase diagrams of our model of ribosome traffic [36] in spaces spanned by three parameters which, for different diagrams, are selected from α, β, the availability of amino-acid monomers, and the rate of GTP hydrolysis. Compared to the two-dimensional phase diagram of the TASEP-type models of ribosome traffic, these three-dimensional phase diagrams provide deeper insight into the interplay of single-ribosome mechanochemistry and their collective spatiotemporal organization.

Trafficlike collective movements of ribosomes on a mRNA track during translation of a gene was demonstrated many years ago by electron microscopy [37]. However, to our knowledge, no attempt has been made so far to study the phase diagram of ribosome traffic by systematic quantitative measurements. But, in contrast to most of the earlier works, we have used experimentally controllable parameters to plot the phase diagrams. Therefore, we hope this paper will stimulate experimental studies of the phase diagrams by systematically varying the supply of amino acids (monomeric subunits of protein) and GTP molecules (fuel of ribosomes) in the solution.

The paper is organized as follows. In Sec. II, we introduce the model of the mechanochemical cycle of individual ribosomes. The exact dwell time distribution is calculated in Sec. III, while the mean-dwell time and the physical interpretations of the Michaelis-Menten-like equation are presented in Sec. IV. The connection between the mean-dwell time and average velocity of a ribosome is pointed out in Sec. V, where we also show the trends of variation of the force-velocity relation with variation of some key parameters of the model. The variance of the dwell time distribution and the diffusion constant of a ribosome are quantitative measures of fluctuations; the analytical expressions of these quantities are presented in Sec. VI, where their relationships are pointed out. The distribution of the run times of the ribosomes on their track and the relation of its first two moments with the corresponding moments of the dwell time distribution are discussed in Sec. VII. The effects of steric interactions among the ribosomes during their trafficlike collective movement on a single mRNA track are studied in Sec. VIII; the overall rates of protein synthesis are presented in Sec. VIII A while in Sec. VIII B, we plot the three-dimensional (3D) phase diagrams of the model and also depict two-dimensional (2D) projections to compare to the corresponding 2D phase diagrams of the TASEP. Finally, the results are summarized and main conclusions are drawn in Sec. IX.

II. MODEL OF MECHANOCHEMICAL CYCLE OF RIBOSOME

Figure 1 depicts the mechanochemical cycle of each ribosome in the stage of elongation of the protein where the integer index j labels the codons on the mRNA track. The amino-acid monomers are supplied to the ribosome in a form in which they form a complex with an adapter molecule called tRNA; the complex is called aminoacyl-tRNA (aatRNA). Each "charged" aatRNA, bound to another protein called EF-Tu, arrives at the ribosome from the surrounding medium. The arrival of the correct aatRNA-EF-Tu, as dictated by the mRNA template, and its recognition by the ribosome located at the site j triggers transition from the chemical state 1 to 2 in the same location with a transition rate ω_a. However, if the aatRNA does not belong to the correct species, it is rejected, thereby causing the reverse transition from state 2 to state 1 with transition rate ω_p. Hydrolysis of GTP drives the transition from state 2 to state 3 with the corresponding rate ω_{h1}. Release of the phosphate group, a product of the GTP hydrolysis, is responsible for the transition from state 3 to state 4; the corresponding rate constant is

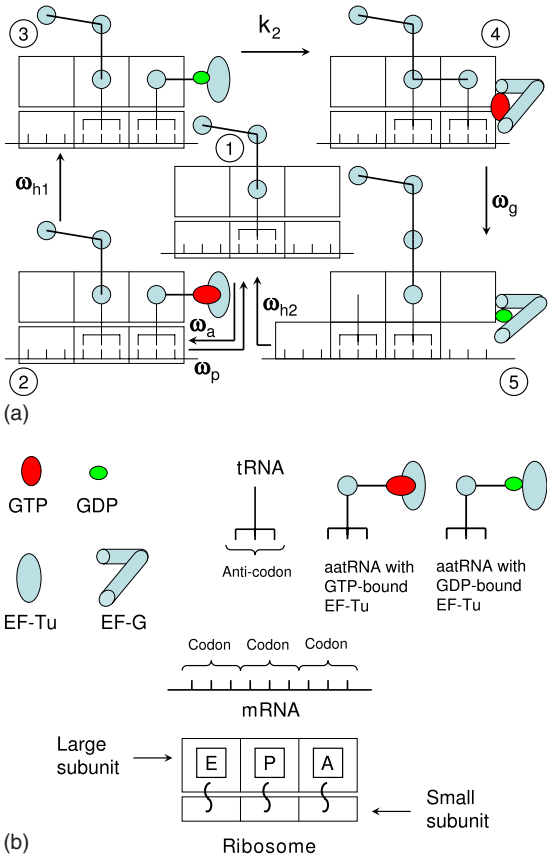

FIG. 1. (Color online) (a) A cartoon for pictorial depiction of the mechanochemical cycle of an individual ribosome in our model. Some of the symbols are explained in (b).

k_2. The peptide bond formation between the newly arrived amino-acid monomer and the growing protein, which leads to the elongation of the protein by one amino-acid monomer (and some associated biochemical processes, including the arrival of the protein EF-G), is captured by the next transition to the state 5 with transition rate ω_g. All the subsequent processes, including the forward translocation of the ribosome by one codon, driven by the hydrolysis of another GTP molecule, and the exit of a naked tRNA from the ribosome complex are captured by a single effective transition from state 5 at site j to the state 1 at the site $j+1$ with the transition rate ω_{h2}. The essential processes of the cycle are summarized in the simplified Fig. 2. More detailed explanations of the states and the transitions are given in Ref. [36].

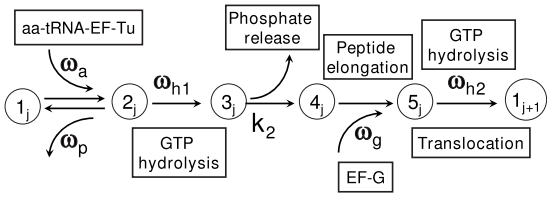

FIG. 2. Mechanochemical cycle of an individual ribosome shown in Fig. 1 is redrawn for the convenience of formulation of the master equations.

III. DWELL TIME DISTRIBUTION FOR A SINGLE RIBOSOME: MOST GENERAL CASE

Because of recent improvements in experimental techniques, it has become possible to image and manipulate single ribosomes [6,15–21]. In the recent experiments on single-ribosome manipulation [6], the distribution of the dwell times of a single ribosome at a codon was measured. It was also shown that the experimental data fit best to a difference of two exponentials. More recently, we [38] have demonstrated that the numerical data obtained from computer simulations of our model can also be fitted to a difference of two exponentials. In this section, we derive an exact analytical formula for the dwell time distribution in our model and compare it to the corresponding numerical data obtained from computer simulations. This analytical formula shows how the distribution of the dwell times can be controlled by tuning the rates of the various substeps of a mechanochemical cycle of the ribosome. This is a new prediction which, in principle, can be tested by repeating the *in vitro* single-ribosome experiments [6] for different concentrations of GTP and aatRNA molecules.

For every ribosome, the dwell time is measured by an imaginary "stopwatch" which is reset to zero whenever the ribosome reaches the chemical state 1, *for the first time*, after arriving at a new codon (say, $j+1$th codon from the jth codon). For the convenience of mathematical formulation and for later comparison to the corresponding results of single molecule enzymatic kinetics, we make the following assumption: a ribosome finds itself in an excited state 1^* following the transition from the state $(j,5)$ to $(j+1,1^*)$ and, then, relaxes to its normal state $(j+1,1)$ with a rate constant δ. If the ribosome relaxes very rapidly from the state 1^* to the state 1, we can set $\delta \to \infty$ at the end of the calculation.

Let $P_\mu(j,t)$ be the probability of finding a ribosome at site j in the chemical state μ at time t. For our calculations in this section, we do not need to write the site index j explicitly. The time evolutions of the probabilities $P_\mu(t)$ are given by

$$\frac{dP_1(t)}{dt} = -\omega_a P_1(t) + \omega_p P_2(t), \tag{1}$$

$$\frac{dP_2(t)}{dt} = \omega_a P_1(t) - (\omega_p + \omega_{h1}) P_2(t), \tag{2}$$

$$\frac{dP_3(t)}{dt} = \omega_{h1} P_2(t) - k_2 P_3(t), \tag{3}$$

$$\frac{dP_4(t)}{dt} = k_2 P_3(t) - \omega_g P_4(t), \tag{4}$$

$$\frac{dP_5(t)}{dt} = \omega_g P_4(t) - \omega_{h2} P_5(t), \tag{5}$$

$$\frac{dP_{1^*}(t)}{dt} = \omega_{h2} P_5(t). \tag{6}$$

The probability that addition of a new amino-acid subunit to the growing protein is completed between times t and $t+\Delta t$ is $f(t)\Delta t$. But,

$$f(t)\Delta t = \Delta P_{1^*}(t) = \omega_{h2} P_5(t)\Delta t, \tag{7}$$

where $\Delta P_{1^*}(t)$ is the probability that the ribosome is in the state 1^* in the time interval between t and $t+\Delta t$. Therefore,

$$f(t) = \frac{dP_{1^*}(t)}{dt} = \omega_{h2} P_5(t). \tag{8}$$

Solving the Eqs. (1)–(6), subject to the normalization condition

$$P_1(t) + P_2(t) + P_3(t) + P_4(t) + P_5(t) + P_{1^*}(t) = 1 \tag{9}$$

and the initial conditions

$$P_1(0) = 1, P_2(0) = P_3(0) = P_4(0) = P_5(0) = P_{1^*}(0) = 0, \tag{10}$$

we get the time-dependent probabilities $P_\mu(t)(\mu = 1, 2, \ldots, 5)$; the details are given in the Appendix. Then, using the relation (8), we obtain the distribution $f(t)$ of the dwell times to be

$$f(t) = C_1 \exp(-\omega_1 t) + C_2 \exp(-\omega_2 t) + C_3 \exp(-k_2 t) + C_4 \exp(-\omega_g t) + C_5 \exp(-\omega_{h2} t), \tag{11}$$

where

$$C_1 = \frac{\omega_a \omega_{h1} k_2 \omega_g \omega_{h2}}{(\omega_2 - \omega_1)(k_2 - \omega_1)(\omega_g - \omega_1)(\omega_{h2} - \omega_1)}, \tag{12}$$

$$C_2 = \frac{\omega_a \omega_{h1} k_2 \omega_g \omega_{h2}}{(\omega_1 - \omega_2)(k_2 - \omega_2)(\omega_g - \omega_2)(\omega_{h2} - \omega_2)}, \tag{13}$$

$$C_3 = \frac{\omega_a \omega_{h1} k_2 \omega_g \omega_{h2}}{(\omega_1 - k_2)(\omega_2 - k_2)(\omega_g - k_2)(\omega_{h2} - k_2)}, \tag{14}$$

$$C_4 = \frac{\omega_a \omega_{h1} k_2 \omega_g \omega_{h2}}{(\omega_1 - \omega_g)(\omega_2 - \omega_g)(k_2 - \omega_g)(\omega_{h2} - \omega_g)}, \tag{15}$$

$$C_5 = \frac{\omega_a \omega_{h1} k_2 \omega_g \omega_{h2}}{(\omega_1 - \omega_{h2})(\omega_2 - \omega_{h2})(k_2 - \omega_{h2})(\omega_g - \omega_{h2})}, \tag{16}$$

and

$$\omega_1 = \frac{\omega_{h1} + \omega_p + \omega_a}{2} - \left[\sqrt{\frac{(\omega_{h1} + \omega_p + \omega_a)^2}{4} - \omega_a \omega_{h1}} \right], \tag{17}$$

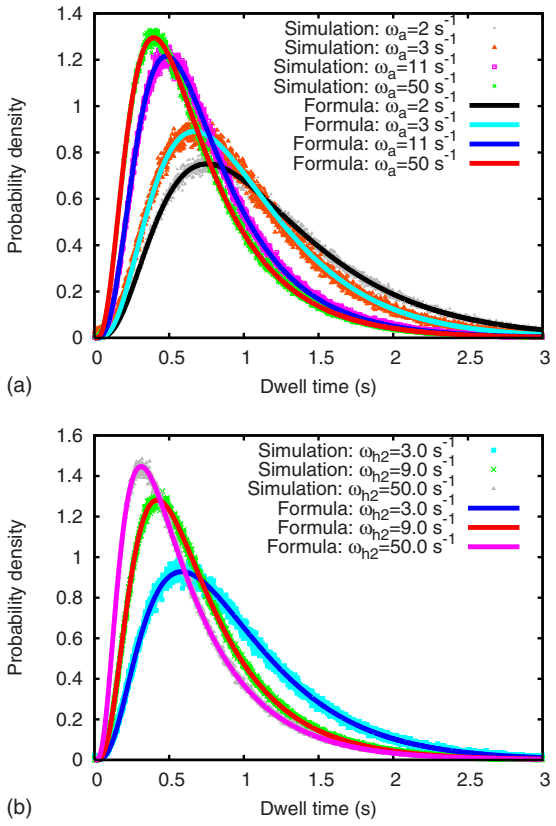

FIG. 3. (Color online) Probability density $f(t)$ of the dwell times of a single ribosome in the most general case of our model for a few different values of (a) the parameter ω_a (which is proportional to the concentration of tRNA-bound amino-acid subunits) and (b) the parameter ω_{h2} (which determines the rate of "stepping"). The continuous curve corresponds to the analytically derived expression (11) whereas the discrete data points have been obtained from computer simulation of the same model.

$$\omega_2 = \frac{\omega_{h1} + \omega_p + \omega_a}{2} + \left[\sqrt{\frac{(\omega_{h1} + \omega_p + \omega_a)^2}{4} - \omega_a \omega_{h1}} \right]. \tag{18}$$

The explicit mathematical formula (11) for the dwell time distribution, which we report in this paper, predicts how the distribution depends quantitatively on the rates of the steps in the mechanochemical cycle of a ribosome. These predictions can be tested by repeating the experiments of Wen *et al.* [6] with different concentrations of amino-acid subunits of the proteins (i.e., aatRNA molecules), fuel of ribosome motor (i.e., GTP molecules), and ribosomes.

We plot the distribution (11) in Fig. 3 and compare it to the corresponding distribution which we have obtained by direct computer simulation of our model. The agreement between the theoretical formula (11) and the simulation data is excellent. Note that $\Sigma_{\mu=1}^{5} C_\mu = 0$, which implies that $f(t)=0$ at $t=0$. Moreover, the nonmonotonic variation of $f(t)$ with t arises from the fact that not all of the coefficients C_μ are positive. As ω_a *decreases* (i.e., effectively, aatRNA becomes more scarce), the tail of the distribution becomes longer and the peak shifts to longer dwell times. Moreover, similar trend

is observed also in the variation of the most probable dwell time with the decrease of ω_{h2}. The trend of variation of the width of the distribution will be discussed later in Sec. VI of this paper.

A. Special case I: $\omega_p=0$

In the special case $\omega_p=0$,

$$f(t) = C_1' \exp(-\omega_a t) + C_2' \exp(-\omega_{h1} t) + C_3' \exp(-k_2 t) + C_4' \exp(-\omega_g t) + C_5' \exp(-\omega_{h2} t), \quad (19)$$

where C_μ' is obtained from C_μ by replacing ω_1 and ω_2 by ω_a and ω_{h1}, respectively. The form of the expression (19) of $f(t)$ makes the underlying physics very transparent—$f(t)$ is a superposition of five different terms each of which decays exponentially with one of the five rate constants. Moreover, a clear pattern in the factors in the denominators of the coefficients $C_\mu'(\mu=1,2,\ldots,5)$ has also emerged.

B. Special case II: $\omega_a=\omega_{h1}=k_2=\omega_g=\omega_{h2}, \omega_p=0$

Note that we have derived the general expression (11) for $f(t)$ assuming that no two rate constants are equal. One can envisage several different possible situations where two or more rate constants have identical numerical values [39]. In order to demonstrate that the form of $f(t)$ can get modified under such special conditions, in this section we consider a very special case where $\omega_p=0$ and all the nonvanishing rate constants are equal, i.e., $\omega_a=\omega_{h1}=\omega_{h2}=\omega_g=k_2=g$. In this case the master equations become much simpler and the expression for $f(t)$ simplifies to the gamma distribution

$$f(t) = \frac{g^k t^{k-1} e^{-gt}}{\Gamma(k)}, \quad (20)$$

where $\Gamma(k)$ is the gamma function with $k=5$.

IV. MEAN DWELL TIME: MICHAELIS-MENTEN EQUATION?

Using the expression for $f(t)$ in

$$\langle t \rangle = \int_0^\infty t f(t) dt, \quad (21)$$

we get the mean-dwell time

$$\langle t \rangle = \frac{C_1}{\omega_1^2} + \frac{C_2}{\omega_2^2} + \frac{C_3}{k_2^2} + \frac{C_4}{\omega_g^2} + \frac{C_5}{\omega_{h2}^2}. \quad (22)$$

Further simplification gives

$$\langle t \rangle = \frac{1}{\omega_a}\left(1 + \frac{\omega_p}{\omega_{h1}}\right) + \frac{1}{\omega_{h1}} + \frac{1}{k_2} + \frac{1}{\omega_g} + \frac{1}{\omega_{h2}}, \quad (23)$$

which is, indeed, the sum of the average time periods spent in different steps of the mechanochemical cycle.

Next we express the "pseudo"-first-order rate constant ω_a as $\omega_a=\omega_a^0[\mathrm{tRNA}]$, where [tRNA] is the concentration of the tRNA molecules. Then, the Eq. (23) can be recast as

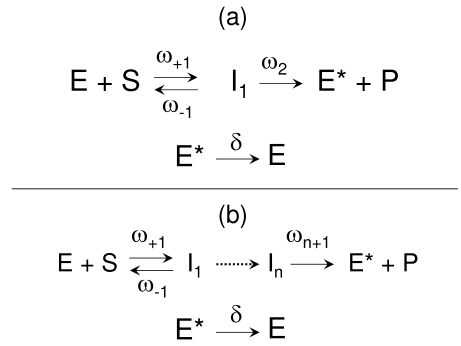

FIG. 4. (a) Catalytic cycle of an enzyme in the Michaelis-Menten theory. E denotes the enzyme while S and P denote the substrate and product, respectively. The symbol I_1 represents the intermediate state of molecular complex of which the enzyme is a component. (b) Generalization of the cycle shown in (a) to n number of intermediate states $I_1,\ldots,I_n$.

$$\langle t \rangle = \frac{1}{V_{\max}} + \left(\frac{K_M}{V_{\max}}\right)\frac{1}{[\mathrm{tRNA}]}, \quad (24)$$

where

$$\frac{1}{V_{\max}} = \frac{1}{\omega_{h1}} + \frac{1}{k_2} + \frac{1}{\omega_g} + \frac{1}{\omega_{h2}} = \frac{1}{\omega_2^{eff}} \quad (25)$$

and

$$K_M = \frac{\omega_2^{eff} + \omega_{-1}^{eff}}{\omega_a^0}, \quad (26)$$

with

$$\omega_{-1}^{eff} = \omega_p\left(\frac{\omega_2^{eff}}{\omega_{h1}}\right). \quad (27)$$

One remarkable feature of the expression (24) is that it is very similar to the Michaelis-Menten (MM) equation for the speed of enzymatic reactions in bulk [12]. In chemical kinetics, the MM equation is derived for the enzymatic cycle shown in Fig. 4 where the enzyme E enhances the rate of the reaction that converts the substrates S into the product P. In that case, the maximum rate of the reaction is given by $V_{\max}=\omega_2$ while the Michaelis constant is $(\omega_{+2}+\omega_{-1})/\omega_{+1}$.

The steps of the mechanochemical cycle of an individual ribosome, as redrawn in Fig. 5, are very similar to those of the generalized MM-like enzymatic cycle shown in Fig. 4(b). The fact that the mean-dwell time for the ribosomes follows

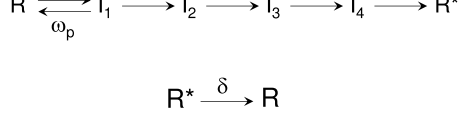

FIG. 5. The mechanochemical cycle of a ribosome, shown in the Fig. 2, is redrawn for the convenience of comparison to the MM enzymatic reaction scheme shown in Fig. 4(b). The symbols I_1,I_2,I_3,I_4 denote the five intermediate states which we labeled in Fig. 2 by the integers 1, 2, 3, 4, respectively.

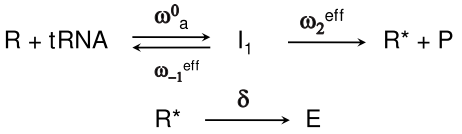

FIG. 6. The effective mechanochemical cycle of a ribosome, where the effective rate constants ω_2^{eff} and ω_{-1}^{eff} are given by the Eqs. (25) and (27), respectively.

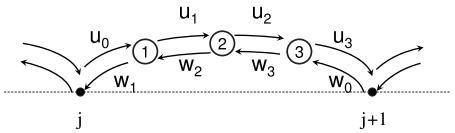

FIG. 7. The mechanochemical cycle of the molecular motor in the Fisher-Kolomeisky model for $m=4$. The horizontal dashed line shows the lattice which represents the track; j and $j+1$ represent two successive binding sites of the motor. The circles labeled by integers denote different "chemical" states in between j and $j+1$.

a MM-like equation is consistent with the experimental observations in recent years [40–45] that the average rate of an enzymatic reaction catalyzed by a single enzyme molecule is, most often, given by the same MM equation.

For our model, we can interpret $1/\langle t\rangle$ as the average rate at which a protein is synthesized by a ribosome, where aatRNA plays the role of the substrate and the protein elongated by one amino acid is the product. In the limit of effectively infinite supply of tRNA molecules, on the average, time required to complete one cycle would be the sum of the times required to complete the remaining steps of the cycle each of which has been assumed to be completely irreversible. This intuitive expectation for the maximum speed of protein synthesis is consistent with the analytical form Eq. (25) of $V_{\max}$. Furthermore, in the expression (26) for the Michaelis constant, the effective rate constants ω_{-1}^{eff} and ω_2^{eff} are the counterparts of ω_{-1} and ω_2, respectively, of Fig. 4(a). Therefore, as far as the average speed is concerned, the actual mechanocycle, shown in Fig. 5, for a single ribosome can be replaced by the simpler MM-like cycle shown in Fig. 6, where ω_a^0 is the counterpart of ω_{+1}, In the limit $k_2 \to \infty$, $\omega_g \to \infty$, $\omega_{h2} \to \infty$, the mechanochemical cycle of a ribosome in our model reduces to the enzymatic cycle shown in Fig. 4(a). In this limit, $\omega_2^{eff} \to \omega_{h1}$ and, hence, the expressions (25) and (26) reduce to the corresponding expressions for $V_{\max}$ and K_M in the MM equation for enzymes.

In reality, however, a ribosome itself is a ribonucleoprotein complex that is not an enzyme, but provides a platform where several distinct catalysts catalyze the respective specific reactions. For example, the GTPases enhance hydrolysis of GTP molecules while the peptidyl transferase catalyzes the formation of the peptide bond between the incoming amino-acid monomer and the growing polypeptide.

A. Comparison to some earlier works

Our derivation of the MM-like equation is different from the derivation of MM-like equation for cytoskeletal motors reported in Ref. [46] where the dwell time distribution was not derived. By making one-to-one correspondence between the mechanochemical cycle in their generic model for cytoskeletal motors and that in our model of ribosome, we find that the MM-like equation reported by Keller and Bustamante [46] reduces to the MM-like Eq. (24).

In a recent work, Jackson *et al.* [47] modeled the process of translation as an enzymatic reaction. However, there are crucial differences between their formulation of translation and our interpretation of the mechanochemical cycle in our model. In their formulation, Jackson *et al.* [47] treated the completely synthesized protein as the product of the enzymatic reaction, i.e., the run of a single ribosome from the initiation site to the termination site was treated as a single enzymatic reaction. In contrast, translocation of a ribosome from one codon to the next and the associated elongation of the growing polypeptide by one amino acid have been treated in our calculation here as a single enzymatic reaction.

V. FORCE-VELOCITY RELATION

Utilizing an earlier result of Derrida [48], Fisher and Kolomeisky proposed a general formula for the average velocity $\langle V\rangle$ of a generic model of molecular motor where the mechanochemical transitions form unbranched cycles. Each cycle consists of m intermediate "chemical" states in between the successive positions on the track of the motor (Fig. 7). The forward transitions take place at rates u_j whereas the backward transitions occur with the rates w_j. Choosing the unit of length to be the separation between the successive equispaced positions of the motor on the track, the average velocity $\langle V\rangle$ of the motor is given by [13]

$$V = \frac{1}{R_m}\left[1 - \prod_{j=0}^{m-1}\left(\frac{w_j}{u_j}\right)\right], \tag{28}$$

where

$$R_m = \sum_{j=0}^{m-1} r_j = \sum_{j=0}^{m-1}\left(\frac{1}{u_j}\right)\left[1 + \sum_{k=1}^{m-1}\prod_{i=1}^{k}\left(\frac{w_{j+i}}{u_{j+i}}\right)\right]. \tag{29}$$

Formally, our model of ribosome is a special case of the Fisher-Kolomeisky model where $u_0=\omega_a$, $u_1=\omega_{h1}$, $u_2=k_2$, $u_3=\omega_g$, $u_4=\omega_{h2}$, and $w_1=\omega_p$. Hence, in this special case, Eq. (28) can be written in a compact form as

$$V = \frac{\omega_{h2}}{1+\Omega_{h2}}, \tag{30}$$

with

$$\Omega_{h2} = \omega_{h2}/k_{eff} \tag{31}$$

and

$$\frac{1}{k_{eff}} = \frac{1}{\omega_a}\left(1 + \frac{\omega_p}{\omega_{h1}}\right) + \frac{1}{\omega_{h1}} + \frac{1}{k_2} + \frac{1}{\omega_g}. \tag{32}$$

Note that k_{eff}^{-1} is an effective time delay induced by the intermediate biochemical steps in between two successive hoppings of the ribosome from one codon to the next [36]. Interestingly, simplification of the exact expression (23) yields

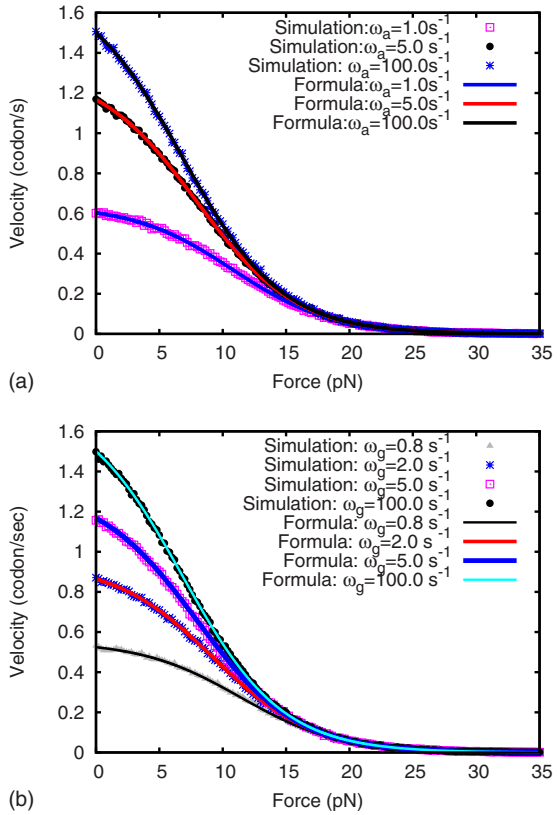

FIG. 8. (Color online) Force-velocity relation for a ribosome in our model for a few different values of the parameter (a) ω_a (which is proportional to the concentration of tRNA-bound amino-acid subunits) and (b) ω_g (which can be controlled by varying GTP concentration). The continuous curve has been obtained from formula (34) whereas the discrete symbols denote the numerical data points obtained from computer simulations of the model.

the same formula (30) which we derived as a special case of the Fisher-Kolomeisky formula for average velocity.

In our model, the load force will only affect the mechanochemical transition from state 5 at j to state 1 at $j+1$. The dependence of the rate constant ω_{h2} on F is given by

$$\omega_{h2}(F) = \omega_{h2}(0)\exp\left(-\frac{F\delta}{k_B T}\right), \tag{33}$$

where $\omega_{h2}(0)$ is the magnitude of the rate constant ω_{h2} in the absence of load force and the typical length of each codon is $\delta = 3 \times 0.34$ nm. Thus, when subjected to a load force F, the force-velocity relation for a single ribosome becomes

$$V(F) = \frac{\omega_{h2}(F)}{1 + \Omega_{h2}(F)}. \tag{34}$$

The force-velocity relation $\langle V\rangle(F)$ has been plotted in Figs. 8(a) and 8(b) for a few different values of ω_a and ω_g, respectively, to demonstrate the dependence of $\langle V\rangle(F)$ on the supply of amino-acid monomers and the chemical fuel GTP. For fixed ω_a and ω_g, $\langle V\rangle$ decreases with increasing F and vanishes at $F = F_s$ which is identified as the corresponding *stall force*. Moreover, for a given F, $\langle V\rangle$ increases monotonically with increasing ω_a and ω_g although the rate of increase gradually slows down. It is interesting to note that F_s is independent of both ω_a and ω_g because, at stall, a ribosome uses neither amino-acid monomers nor GTP. For the typical values of the rate constants, which we have used in Fig. 8, $F_s \simeq 25-27$ pN. This theoretical estimate is consistent with the value 26.5 pN reported by Sinha *et al.* [49].

VI. FLUCTUATIONS: MEAN SQUARE DWELL TIME AND DIFFUSION CONSTANT

A. Fluctuations in dwell times

Mean-square dwell time is defined by

$$\langle t^2\rangle = \int_0^\infty t^2 f(t)dt. \tag{35}$$

For our model,

$$\langle t^2\rangle = 2\left[\frac{C_1}{\omega_1^3} + \frac{C_2}{\omega_2^3} + \frac{C_3}{k_2^3} + \frac{C_4}{\omega_g^3} + \frac{C_5}{\omega_{h2}^3}\right]. \tag{36}$$

Expression (36) can be expressed also as

$$\langle t^2\rangle = 2(\langle t\rangle^2 - \xi_2), \tag{37}$$

where

$$\xi_2 = \left(\frac{\omega_p}{\omega_a\omega_{h1}}\right)\left(\frac{1}{k_2} + \frac{1}{\omega_g} + \frac{1}{\omega_{h2}}\right) + \frac{1}{\omega_a\omega_{h1}} + \frac{1}{\omega_a k_2} + \frac{1}{\omega_a\omega_g} + \frac{1}{\omega_a\omega_{h2}} + \frac{1}{\omega_{h1}k_2} + \frac{1}{\omega_{h1}\omega_g} + \frac{1}{\omega_{h1}\omega_{h2}} + \frac{1}{k_2\omega_g} + \frac{1}{k_2\omega_{h2}} + \frac{1}{\omega_g\omega_{h2}}. \tag{38}$$

Note that only the first term involves ω_p. The remaining ten terms are the inverse of the products of the five rate constants.

Let us define "randomness parameter" r as

$$r = \frac{\langle t^2\rangle - \langle t\rangle^2}{\langle t\rangle^2}. \tag{39}$$

Note that r is a quantitative measure of the fluctuations in the dwell times of a ribosome. By substituting the expressions of $\langle t^2\rangle$ and $\langle t\rangle$ into Eq. (39), we obtain

$$r = \frac{\langle t\rangle^2 - 2\xi_2}{\langle t\rangle^2}. \tag{40}$$

A nontrivial feature of the expression (40) is that it cannot be obtained simply by substituting ω_{-1}^{eff} and ω_2^{eff} into the expression for r derived by Kou *et al.* [42] for the two-step Michaelis-Menten enzymatic reaction. In other words, the fluctuations of the dwell times in the five-step model for the kinetics of ribosomes cannot be captured by the effective two-state model drawn in Fig. 6.

The randomness parameter r is plotted in Fig. 9 as a function of the tRNA concentration for a few different values of the parameters ω_h [in (a)] and ω_p [in (b)]. We find (not shown in any figure) that the numerator of r (i.e., $\langle t^2\rangle - \langle t\rangle^2$)

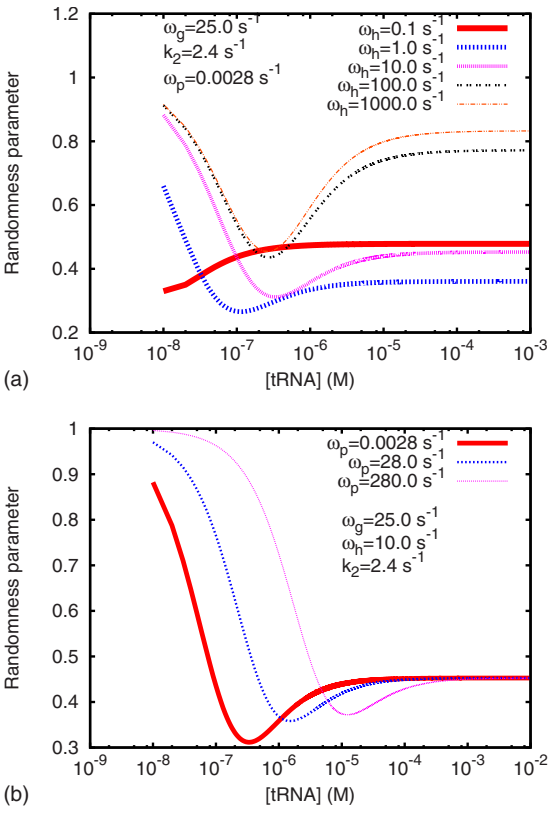

FIG. 9. (Color online) The randomness parameter r, defined by Eq. (39), is plotted against the concentration of aatRNA for a few different values of ω_h [in (a)] and ω_p [in (b)].

decreases monotonically with increasing concentration of tRNA; it is the variation of the denominator of r with tRNA concentration that is responsible for the nonmonotonic variation of r.

It is well known [42] that, for a one-step Poisson process, $r=1$. At extremely low concentrations of aatRNA, the binding of a correct species of aatRNA to the A site on the large subunit of a ribosome is the rate-limiting step in its mechanochemical cycle. Therefore, r is unity at sufficiently low values of aatRNA. r decreases with the increase of aatRNA concentration. This decrease is caused by the formation of intermediate complexes which also affect the rates of progress of the mechanochemical cycle. However, with the further increase of aatRNA concentration, the randomness parameter r increases again. Finally, randomness parameter saturates to a value which is determined by the number of rate-limiting steps in the mechanochemical cycle. Such nonmonotonic variation of r with aatRNA concentration reduces to a monotonic decrease when the magnitudes of the rate constants are sufficiently high (see Fig. 10).

B. Diffusion constant

The diffusion constant D is a measure of fluctuations around the directed movement of the ribosome, on the average, in space. We now derive a closed-form expression for D and relate it to the fluctuations in the dwell times. Fisher and Kolomeisky's general result for diffusion coefficient D is

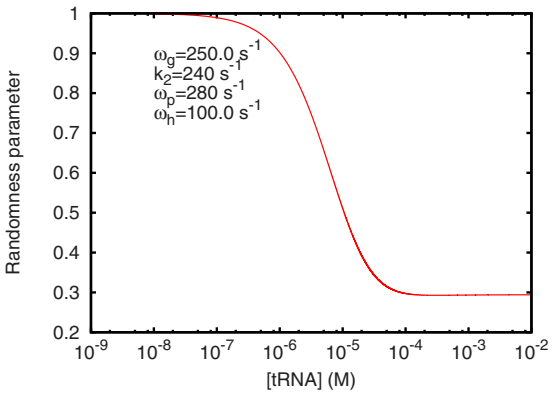

FIG. 10. (Color online) The randomness parameter r, defined by Eq. (39), is plotted against the concentration of aatRNA for a set of parameter values where all the magnitudes of all the rate constants, other than ω_a, are quite high.

$$D = \left[\frac{(VS_N + dU_N)}{R_N^2} - \frac{(N+2)V}{2}\right]\frac{d}{N}, \tag{41}$$

where

$$S_N = \sum_{j=0}^{N-1} s_j \sum_{k=0}^{N-1} (k+1) r_{k+j+1} \tag{42}$$

and

$$U_N = \sum_{j=0}^{N-1} u_j r_j s_j, \tag{43}$$

while

$$s_j = \frac{1}{u_j}\left(1 + \sum_{k=1}^{N-1}\prod_{i=1}^{k}\frac{w_{j+1-i}}{u_{j-i}}\right), \tag{44}$$

$$R_N = \sum_{j=0}^{N-1} r_j, \tag{45}$$

In our units $d=1$. Therefore, in our model, the expression for D becomes

$$D = (\langle t\rangle^2 - 2\xi_2)/2\langle t\rangle^3. \tag{46}$$

Finally, we observe that r, which is a measure of the fluctuations in the dwell times, is related to D and $\langle V\rangle$ by [50],

$$r = \frac{2D}{\langle V\rangle}. \tag{47}$$

VII. DISTRIBUTION OF RUN TIMES

In this section, we report the distribution of the run times τ of an individual from the start codon to the stop codon. The run time is related to the dwell times by the relation

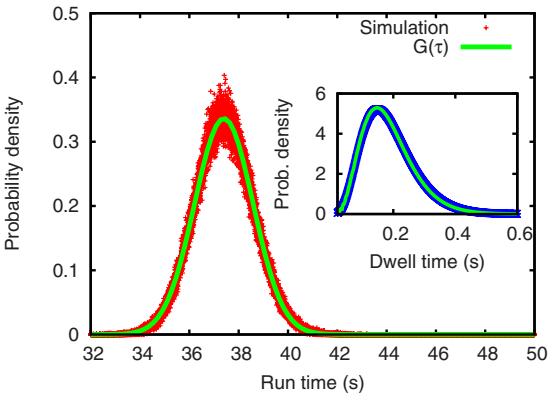

FIG. 11. (Color online) Distribution of the run times of a ribosome in our model. The continuous curve is the Gaussian distribution predicted by our theory while the discrete data points have been obtained from computer simulations. Inset shows the dwell time distribution for the same set of parameter values.

$$\tau = \sum_{j=1}^{L} t_j. \tag{48}$$

Central limit theorem states that, as $L \to \infty$, the distribution $G(\tau)$ of the run times τ approaches a Gaussian, irrespective of the nature of the distribution of the dwell times, since the dwell times at different codons are independent of each other. Obviously, for sufficiently large L [51],

$$G(\tau) = \frac{1}{\sqrt{(2\pi\sigma_\tau^2)}} \exp\left(-\frac{(\tau - \langle\tau\rangle)^2}{2\sigma_\tau^2}\right), \tag{49}$$

where

$$\langle\tau\rangle = L\langle t\rangle \tag{50}$$

and

$$\langle\tau^2\rangle - \langle\tau\rangle^2 = L(\langle t^2\rangle - \langle t\rangle^2). \tag{51}$$

Using $\langle t\rangle$ from Eq. (23) and $\langle t^2\rangle$ from Eq. (37), we obtain the Gaussian distribution $G(\tau)$. The Gaussian distribution $G(\tau)$ thus obtained is plotted in Fig. 11; it is in excellent agreement with the corresponding numerical data obtained from computer simulations.

VIII. EFFECTS OF STERIC INTERACTIONS OF RIBOSOMES

The average velocity of a ribosome is also the mean rate of polymerization of a protein. We define the *flux* of ribosomes to be the total number of ribosomes leaving the stop codon (i.e., $j=L$) per unit time. Obviously, the overall rate of protein synthesized from a single mRNA template is identical to the flux of the ribosomes on that mRNA track. The *number density* of the ribosomes is given by $\rho = N/L$. The size of a typical ribosome is such that, simultaneously, it covers ℓ codons, where $\ell \gg 1$. We treat ℓ as a parameter of the model. For a given number N of ribosomes, the total fraction of the lattice covered by all the ribosomes is given by the *coverage density* $\rho_{cov} = N\ell/L$.

In the preceding sections, we have ignored the possibility of steric interactions among the ribosomes. Consequently, the average velocity was independent of the ribosome population on the given mRNA track. Such a scenario holds at most at sufficiently low coverage densities. However, in the presence of inter-ribosome interactions, the average velocity becomes a function of the coverage density thereby giving rise to nontrivial variation of the flux J (and, hence, the overall rate of protein synthesis) with ρ_{cov}. Moreover, the density profile of the ribosomes on the track also exhibits interesting features. In this section, we study the spatiotemporal organization of the ribosomes in terms of the flux as well as the density profiles on a single mRNA track and plot the phase diagrams of the model.

Let $P_\mu(j,t)$ be the probability of finding a ribosome at site j, in the chemical state μ at time t. Also, $P(j,t) = \Sigma_{\mu=1}^{5} P_\mu(j,t)$ is the probability of finding a ribosome at site j, irrespective of its chemical state. Let $P(j|k)$ be the conditional probability that, given a ribosome at site j, there is another ribosome at site k. Then, $Q(j|k) = 1 - P(j|k)$ is the conditional probability that, given a ribosome in site j, site k is empty. In the mean-field approximation, the master equations for the probabilities $P_\mu(j,t)$ are given by [36]

$$\frac{\partial P_1(j,t)}{\partial t} = \omega_{h2} P_5(j-1,t) Q(j-1|j-1+\ell) + \omega_p P_2(j,t) - \omega_a P_1(j,t), \tag{52}$$

$$\frac{\partial P_2(j,t)}{\partial t} = \omega_a P_1(j,t) - (\omega_p + \omega_{h1}) P_2(j,t), \tag{53}$$

$$\frac{\partial P_3(j,t)}{\partial t} = \omega_{h1} P_2(j,t) - k_2 P_3(j,t), \tag{54}$$

$$\frac{\partial P_4(j,t)}{\partial t} = k_2 P_3(j,t) - \omega_g P_4(j,t), \tag{55}$$

$$\frac{\partial P_5(j,t)}{\partial t} = \omega_g P_4(j,t) - \omega_{h2} P_5(j,t) Q(j|j+\ell). \tag{56}$$

Because of the normalization condition

$$P(j,t) = \sum_{\mu=1}^{5} P_\mu(j,t) = \frac{N}{L} = \rho, \tag{57}$$

not all of the five $P_\mu(j,t)$ are independent.

A. Effects of steric interactions on rate of protein synthesis

The dwell time distribution $f(t)$ certainly gets affected by the steric interactions. As a first step, we have calculated the effects of the interactions on the average velocity which is just the inverse of the mean-dwell time.

Under periodic boundary conditions, in the steady state, $P_\mu(j,t)$ become independent of j and t. From the steady-state limit of the Eqs. (52)–(56), we derived the expressions $P_\mu(\mu=1,2,\ldots,5)$ and the flux [36]

$$J_{\mathrm{PBC}} = \rho\langle V\rangle = \frac{\omega_{h2}\rho(1-\rho l)}{(1+\rho-\rho l)+\Omega_{h2}(1-\rho l)}, \tag{58}$$

where

$$\Omega_{h2} = \omega_{h2}/k_{eff} \tag{59}$$

and k_{eff} is given by Eq. (32).

From Eq. (58), the ρ-dependent average velocity $\langle V\rangle$ can be obtained by dividing J by ρ. At sufficiently low densities, this expression reduces to

$$J = \frac{\omega_{h2}\rho}{(1+\Omega_{h2})} \tag{60}$$

and, hence, we recover the exact formula (30) for the average velocity of a single ribosome.

B. Phase diagrams under open boundary conditions

Initiation and termination of protein synthesis are captured more realistically by imposing open boundary conditions (OBC) than by the periodic boundary conditions (PBC). Whenever the first ℓ sites on the mRNA are vacant, this cluster of sites is allowed to be covered by a fresh ribosome with the probability α in the time interval Δt (in all our numerical calculations we take $\Delta t=0.001$ s). Since α is the probability of initiation in time Δt, the corresponding rate constant (i.e., probability of initiation per unit time) ω_α is related to α by $\alpha=1-e^{-\omega_\alpha \Delta t}$. Similarly, whenever the rightmost ℓ sites of the mRNA lattice are covered by a ribosome, i.e., the ribosome is bound to the Lth codon, the ribosome gets detached from the mRNA with probability β in the time interval Δt; the corresponding rate constant being denoted by ω_β. For all further discussions in this paper, we will assume $\omega_{h1}=\omega_{h2}=\omega_h$ because both of these processes are driven by GTP hydrolysis.

TASEP is known to exhibit three dynamical phases, namely, high-density (HD) phase, low-density (LD) phase, and the maximal current (MC) phase in the α-β plane. Our main interest is to explore the nature of the dynamical phases in different regions of the four-dimensional space spanned by α, β, P_{ω_a}, and P_{ω_h}.

The parameters ω_a and ω_h can be controlled by varying the concentrations of the aatRNA molecules and GTP molecules in the solution. The parameter α is determined by the rate of assembling of the large and small subunits of a ribosome, their final coupling on the initiation site, and the assistance of several other regulatory proteins in the initiation of the actual polymerization of a protein. Strictly speaking, a single parameter β captures essentially two different events both of which take place at the termination site $j=L$. After the full protein has been polymerized, the ribosome releases the protein into the surrounding medium and then dissociates from the mRNA track (the decoupling of the two subunits also takes place; these are then recycled for another round of protein synthesis) [52,53]. Therefore, the value $\beta=1$, which we assumed in Ref. [36] is, in general, not very realistic. Even in the special case $\beta=1$, in Ref. [36], we reported only a couple of two-dimensional cross sections of the full phase diagram of this model. In this paper, we plot phase diagrams in three-dimensional spaces spanned by $\alpha-\beta-P_{\omega_a}$ and $\alpha-\beta-P_{\omega_h}$.

For plotting the phase diagram, we use the same extremum principle [54–57] which we used in Ref. [36]. In this approach, we imagine that the left and right boundaries of the system are connected to two reservoirs with particle densities ρ_- and ρ_+, respectively. These two reservoirs are essentially two infinite lattices with the number densities ρ_- and ρ_+, respectively. We calculate the unknown densities ρ_- and ρ_+, in terms of the rate constants of our model, by imposing the requirement that these reservoirs give rise to the same probabilities α and β of hopping with which a ribosome enters and exits, respectively, the open system.

The extremum principle then relates the flux $\mathcal{J}$ in the open system to the flux $J(\rho)$ for the corresponding closed system (i.e., the system with periodic boundary conditions). Extremum current hypothesis [54–57] states that, for the open system connected to the two reservoirs of number densities ρ_- and ρ_+ at its entrance and exit, the flux $\mathcal{J}$ is related to the corresponding flux J_{PBC} in the closed system by

$$\mathcal{J} = \begin{cases} \max J_{\mathrm{PBC}}(\rho) & \text{if } \rho_- > \rho > \rho_+ \\ \min J_{\mathrm{PBC}}(\rho) & \text{if } \rho_- < \rho < \rho_+. \end{cases} \tag{61}$$

Since the flux-density relation (also called the fundamental diagram) of our model of ribosome traffic under periodic boundary conditions exhibits a single maximum, the extremum principle reduces to a simpler maximum current principle (MCP). According to this MCP, in the limit $L\to\infty$,

$$\mathcal{J} = \max J_{\mathrm{PBC}}(\rho) \text{ if } \rho_- > \rho > \rho_+. \tag{62}$$

1. Calculation of ρ_*, ρ_- and ρ_+

From Eq. (58), the maximum flux under PBC corresponds to the number density

$$\rho_* = \sqrt{\left(\frac{1+\Omega_{h2}}{\ell}\right)}\left[\frac{1}{\sqrt{\ell(1+\Omega_{h2})}+1}\right]. \tag{63}$$

Next we calculate ρ_-. We use symbol 1 to represent the sites covered by ribosome while the symbol 0 represents the sites which are not covered by any ribosome. Let P_-^{jump} be the probability that, given an empty site, from left a ribosome will hop onto it in the next time step. We have

$$P_-^{jump} = P(\underbrace{1\ \ldots\ \ldots\ \ldots\ \ldots\ \ldots\ 1}_{\ell}|\,\underline{0})P_5\omega_{h2}\Delta t, \tag{64}$$

where P_5 is the probability of finding ribosome in state 5 inside the reservoir and the conditional probability $P(\underbrace{1\ldots\ldots\ldots\ldots 1}_{\ell}|\,\underline{0})$ represents that, given an empty site,

$$P(\underbrace{1\ \ldots\ \ldots\ \ldots\ \ldots\ \ldots\ 1}_{\ell}|\,\underline{0}) = \frac{\rho}{(1+\rho-\rho\ell)}. \tag{65}$$

Moreover, as argued in Ref. [36],

$$P_5 = \frac{1}{1+\Omega_{h2}}. \tag{66}$$

Now, ρ_- is the solution of the equation $\alpha = P_-^{jump}$ and, hence, we get

$$\rho_- = \frac{\alpha(1+\Omega_{h2})}{\alpha(1+\Omega_{h2})(\ell-1)+P_{\omega_{h2}}}, \tag{67}$$

where $P_{\omega_{h2}}$ is the probability of hydrolysis in time Δt.

Following similar arguments, we now calculate ρ_+. The probability P_+^{jump}, given that a ribosome which covers ℓ successive sites, will hop onto the next adjacent empty site to its right in the next time step,

$$P_+^{jump} = P(\overbrace{1\ldots\ldots\ldots\ldots..1}^{\ell}\,|\,0)P_5P_{\omega_{h2}}, \tag{68}$$

where $P(\overbrace{1\ldots\ldots\ldots\ldots..1}^{\ell}|0)$ is the conditional probability of finding a hole at site j, given that the site $(j-\ell-1)$ is occupied by the leftmost part of the ribosome. It is straightforward to show that

$$P(\overbrace{1\ldots\ldots\ldots\ldots..1}^{\ell}|0) = \frac{1-\rho\ell}{1+\rho-\rho\ell}. \tag{69}$$

Now, ρ_+ is the solution of the equation $\beta = P_+^{jump}$ and, hence, we get

$$\rho_+ = \frac{\beta(1+\Omega_{h2})-P_{\omega_{h2}}}{\beta(1+\Omega_{h2})(\ell-1)-\ell P_{\omega_{h2}}}. \tag{70}$$

In the limit $k_{eff}\to\infty$, the expressions (70) and (67) for ρ_+ and ρ_- reduce to the corresponding expressions $\rho_-=\alpha$ and $\rho_+ = 1-\beta$, respectively, for TASEP.

2. Surface separating LD and MC phases

The MCP imposes the condition

$$\rho_- = \rho_* \tag{71}$$

on the surface which separates the LD and MC phases. Substituting the expressions (67) for ρ_- into Eq. (71), we obtain

$$\alpha = \frac{P_{\omega_{h2}}\rho_*}{(1+\Omega_{h2})[1-\rho_*(\ell-1)]}. \tag{72}$$

3. Surface separating HD and MC phases

From the MCP

$$\rho_* = \rho_+ \tag{73}$$

on the boundary between the HD and MC phases. Using expression (70) for ρ_+, we obtain

$$\beta = \frac{P_{\omega_{h2}}(1-\rho_*\ell)}{(1+\Omega_{h2})[1-\rho_*(\ell-1)]}. \tag{74}$$

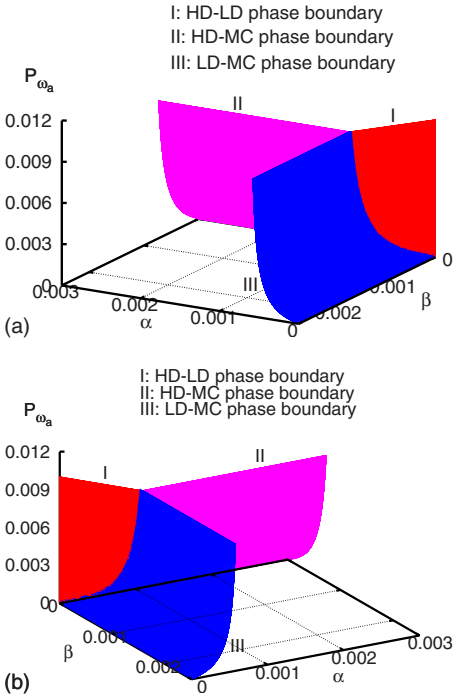

FIG. 12. (Color online) A 3D phase diagram of our ribosome traffic model. The LD and HD phases coexist on the surface I (red). Surfaces II (purple) and III (blue) separate the MC phase from the HD and LD phases, respectively. Phase diagram is shown in (a) and (b) from two different orientations. The parameters used are $\omega_p = 0.0028\ \text{s}^{-1}$, $\omega_a = 25.0$, $k_2 = 2.4\ \text{s}^{-1}$, $\omega_g = 25.0\ \text{s}^{-1}$

4. Surface of coexistence of HD and LD phases

Since the HD and LD phases coexist on the surface separating these two phases, we obtain the boundary by solving the equation

$$J_{\text{PBC}}(\rho_-) = J_{\text{PBC}}(\rho_+) \tag{75}$$

because the same current passes through the two coexisting phases in the steady state, where the density on the entry side is ρ_- and that on the exit side is ρ_+.

Now incorporating the expressions of ρ_- from Eq. (67) and ρ_+ from Eq. (70) into Eq. (58) and using Eq. (75), we find that the equation of the surface of coexistence of LD and HD phases is given by

$$\alpha = \frac{P_{\omega_{h2}}\beta(1+\Omega_{h2})}{P_{\omega_{h2}}\ell+\beta(1-\ell+2\Omega_{h2}-\ell\Omega_{h2}+\Omega_{h2}^2)} \tag{76}$$

or, equivalently,

$$\beta = \frac{\alpha\ell P_{\omega_{h2}}}{(1+\Omega_{h2})(P_{\omega_{h2}}-\alpha+\ell\alpha-\Omega_{h2}\alpha)}. \tag{77}$$

5. Phase diagrams

In Fig. 12 we have plotted a 3D phase diagram of the ribosome traffic model, in the $\alpha-\beta-P_{\omega_a}$ space, which we obtained by following the MCH-based approach explained above. The corresponding 3D phase diagram in the

$\alpha-\beta-P_{\omega_{h2}}$ space is plotted in Fig. 13. The LD and HD phases coexist on the surface I. A first-order phase transition takes place across this surface. Surfaces II and III separate the MC phase from the HD and LD phases, respectively. The 3D phase diagrams plotted in Figs. 12(a) and 13(a) are differently oriented in Figs. 12(b) and 13(b), respectively, to show the regions hidden in Fig. 12(a) and 13(a) behind the surfaces I–III.

By drawing flat surfaces parallel to the $\alpha-\beta$ plane, each corresponding to a fixed value of P_{ω_a} [in (a)] or $P_{\omega_{h2}}$ [in (b)], we have obtained the curves of intersection of this flat plane with surfaces I–III. By projecting these curves on the plane $P_{\omega_{h2}}=0$, we also obtained the 2D phase diagram of the system in the $\alpha-\beta$ plane for several different values of $P_{\omega_{h2}}$. This phase diagram helps in comparing and contrasting our results for the ribosome traffic model with the 2D phase diagram of the TASEP in the $P_{\omega_{h2}}$ plane (Fig. 14). The most interesting feature is that, unlike TASEP, the lines on which HD and LD phases coexist are curved. This characteristic seems to be the general feature of such phases diagrams, rather than an exception; similar curved lines of coexistence between HD and LD phases have been observed also in some other contexts [58].

6. Average density profiles

The bulk density of the system is governed by the following equations:

$$\rho=\begin{cases}\rho_- & \text{if } \beta>\dfrac{\alpha\ell P_{\omega_{h2}}}{(1+\Omega_{h2})(P_{\omega_{h2}}-\alpha+\ell\alpha-\Omega_{h2}\alpha)} \quad \text{and} \quad \alpha<\dfrac{P_{\omega_{h2}}\rho_*}{(1+\Omega_{h2})[1-\rho_*(\ell-1)]} \Rightarrow \text{LD} \\ \rho_+ & \text{if } \beta<\dfrac{P_{\omega_{h2}}(1-\rho_*\ell)}{(1+\Omega_{h2})[1-\rho_*(\ell-1)]} \quad \text{and} \quad \alpha>\dfrac{P_{\omega_{h2}}\beta(1+\Omega_{h2})}{P_{\omega_{h2}}\ell+\beta(1-\ell+2\Omega_{h2}-\ell\Omega_{h2}+\Omega_{h2}^2)} \Rightarrow \text{HD} \\ \rho_* & \text{if } \beta>\dfrac{P_{\omega_{h2}}(1-\rho_*\ell)}{(1+\Omega_{h2})[1-\rho_*(\ell-1)]} \quad \text{and} \quad \alpha>\dfrac{P_{\omega_{h2}}\rho_*}{(1+\Omega_{h2})[1-\rho_*(\ell-1)]} \Rightarrow \text{MC}.\end{cases} \tag{78}$$

IX. SUMMARY AND CONCLUSION

In this paper, we have derived the exact analytical expression for the distribution of the dwell times of ribosomes at each codon on the mRNA track. For this purpose, we have used a model that captures the essential steps in the mechanochemical cycle of a ribosome. As more details of this cycle get unveiled by new experiments, our model can be extended to capture those new features and the dwell time distribution can be recalculated accordingly. Moreover, some of the transitions in the mechanochemical cycle used in our model may require reinterpretation to reconcile with new observations. Nevertheless, at this stage, the dwell time distribution predicted by our theory agrees qualitatively with the corresponding distribution observed *in vitro* single-ribosome experiments. Moreover, our prediction can be tested quantitatively by repeating the single-ribosome experiments varying the supply of amino-acid monomers and GTP molecules.

From the full distribution, we have also calculated the mean-dwell time which satisfies a Michaelis-Menten-like equation. We have pointed out the formal similarities between the cycles, and the corresponding equations, for a single enzyme molecule and a single ribosome, which are responsible for the Michalis-Menten-like form of the mean-dwell time. The inverse of the mean-dwell time is also the average velocity of the ribosome. The expression of this average velocity obtained from the dwell time distribution is identical to that obtained by an alternative approach pioneered by Fisher and Kolomeisky in the context of generic models of molecular motors. Finally, following standard procedure, we capture the effects of load force by modifying the rate constant ω_{h2} and predict the force-velocity relation and its dependence on experimentally controllable parameters. From this relation, we have estimated the stall force of a ribosome. Our theoretical estimate is consistent with the experimentally measured value reported in the literature. However, to our knowledge, the full force-velocity relation for ribosomes has not been measured so far. But, with the rapid progress in the experimental techniques, it should be possible in near future to test the full force-velocity relation predicted by our theory.

We have presented a few quantitative characteristics of the fluctuations in the kinetics of ribosomes. We have defined a "randomness parameter" r, which is a measure of the fluctuations in the dwell times. From the full probability density of the dwell times, we have derived the expression for r and analyzed some of its interesting features. We have also reported the analytical expression for the diffusion constant and related it to the mean velocity and the randomness parameter. Using the central limit theorem, we have argued that the distribution of the run times of the ribosomes from the start codon to the stop codon is Gaussian and also pointed out the relations between its first two moments and those of the dwell time distribution.

To our knowledge, the run time distribution of ribosomes has not been measured so far. RNA polymerase (RNAP)

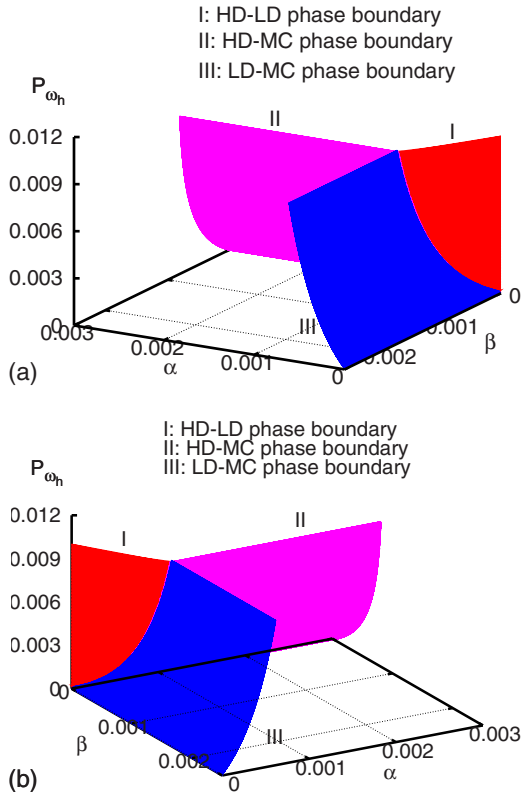

FIG. 13. (Color online) Same as in Fig. 12 except that ω_h has been used instead of ω_a.

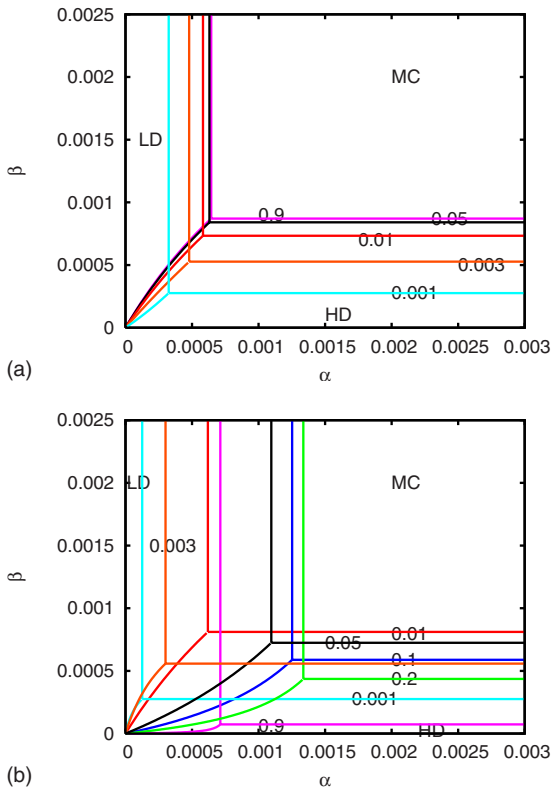

FIG. 14. (Color online) 2D cross sections of the 3D phase diagrams of the ribosome traffic model parallel to the $\alpha-\beta$ plane for different values of (a) P_{ω_a} and (b) P_{ω_h}, all projected onto the same figure. The numbers on the phase boundary lines represent different values of (a) P_{ω_a} and (b) P_{ω_h}. The HD and LD phases coexist on the curved lines whereas the straight lines separate the MC phase from the HD and LD phases, as shown. The parameters used for this figure are $\omega_p=0.0028$ s^{-1}, $\omega_a=25.0$, $k_2=2.4$ s^{-1}, $\omega_g=25.0$ s^{-1}.

motor runs on a DNA track using the track to polymerize the complementary RNA. There are some similarities between template-dictated polymerizations driven by ribosome and RNAP. The run time distribution of RNAP has been measured and found to be Gaussian [59]. This is consistent with the Gaussian run time distribution for ribosomes predicted in this paper which follows from very general arguments based on the central limit theorem.

Incorporating inter-ribosome steric interactions in the model, we have developed a model for ribosome traffic. The model may be regarded as a TASEP for hard rods each of which has five distinct "internal states;" transitions between these internal states constitute parts of the mechanochemical cycle of a ribosome. Initiation and termination of the polymerization of individual proteins are captured by imposing open boundary conditions. For this model, we have drawn three-dimensional phase diagrams in spaces spanned by parameters which can be varied in a controlled manner in laboratory experiments *in vitro*. In principle, the phase diagram can be obtained by analyzing the density profile of the ribosomes in electron micrographs of the system for several different concentrations of amino-acid subunits, GTP concentration, etc.

ACKNOWLEDGMENTS

We thank G. M. Schütz for useful correspondences. This work has been supported by a grant from CSIR (India). Debanjan Chowdhury and T.V.R. thank DST, government of India, for KVPY Foundation and Ramanna Foundation, respectively. A.G. thanks UGC (India) for senior research foundation. T.V.R. would also like to thank National Centre for Biological Sciences, Bangalore, for hospitality.

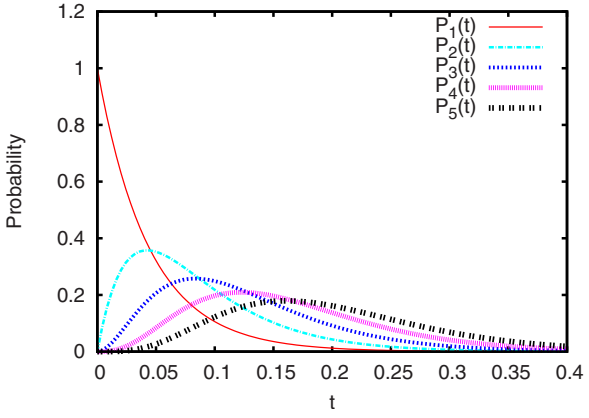

FIG. 15. (Color online) The probabilities $P_\mu(t)$ $(\mu=1,2,\ldots,5)$ corresponding to the initial conditions $P_1(0)=1$ and $P_2(0)=P_3(0)=P_4(0)=P_5(0)=0$ [see Eqs. (79)–(83)] are plotted for the parameter set $\omega_a=23.0$, $\omega_{h1}=24.0$, $k_2=25.0$, $\omega_g=26.0$, $\omega_{h2}=27.0$, and $\omega_p=0.5$.

APPENDIX

The solution of the Eqs. (1) and (6) for the initial condition (10) is given by

$$P_1(t) = \exp(-\omega_a t) + \omega_a \omega_p \left[\frac{\exp(-\omega_1 t)}{(\omega_a - \omega_1)(\omega_2 - \omega_1)} + \frac{\exp(-\omega_2 t)}{(\omega_a - \omega_2)(\omega_1 - \omega_2)} + \frac{\exp(-\omega_a t)}{(\omega_1 - \omega_a)(\omega_2 - \omega_a)} \right], \tag{A1}$$

$$P_2(t) = \omega_a \left[\frac{\exp(-\omega_1 t)}{(\omega_2 - \omega_1)} + \frac{\exp(-\omega_2 t)}{(\omega_1 - \omega_2)} \right], \tag{A2}$$

$$P_3(t) = \omega_a \omega_{h1} \left[\frac{\exp(-\omega_1 t)}{(\omega_2 - \omega_1)(k_2 - \omega_1)} + \frac{\exp(-\omega_2 t)}{(\omega_1 - \omega_2)(k_2 - \omega_2)} + \frac{\exp(-k_2 t)}{(\omega_1 - k_2)(\omega_2 - k_2)} \right], \tag{A3}$$

$$P_4(t) = \omega_a \omega_{h1} k_2 \left[\frac{\exp(-\omega_1 t)}{(\omega_2 - \omega_1)(k_2 - \omega_1)(\omega_g - \omega_1)} + \frac{\exp(-\omega_2 t)}{(\omega_1 - \omega_2)(k_2 - \omega_2)(\omega_g - \omega_2)} + \frac{\exp(-k_2 t)}{(\omega_1 - k_2)(\omega_2 - k_2)(\omega_g - k_2)} + \frac{\exp(-\omega_g t)}{(\omega_1 - \omega_g)(\omega_2 - \omega_g)(k_2 - \omega_g)} \right], \tag{A4}$$

$$P_5(t) = \omega_a \omega_{h1} k_2 \omega_g \left[\frac{\exp(-\omega_1 t)}{(\omega_2 - \omega_1)(k_2 - \omega_1)(\omega_g - \omega_1)(\omega_{h2} - \omega_1)} + \frac{\exp(-\omega_2 t)}{(\omega_1 - \omega_2)(k_2 - \omega_2)(\omega_g - \omega_2)(\omega_{h2} - \omega_2)} + \frac{\exp(-k_2 t)}{(\omega_1 - k_2)(\omega_2 - k_2)(\omega_g - k_2)(\omega_{h2} - k_2)} + \frac{\exp(-\omega_g t)}{(\omega_1 - \omega_g)(\omega_2 - \omega_g)(k_2 - \omega_g)(\omega_{h2} - \omega_g)} + \frac{\exp(-\omega_{h2} t)}{(\omega_1 - \omega_{h2})(\omega_2 - \omega_{h2})(k_2 - \omega_{h2})(\omega_g - \omega_{h2})} \right]. \tag{A5}$$

These distributions are plotted in Fig. 15 for one set of values of the model parameters. These clearly shows that the probability $P_1(t)$ decreases monotonically from the initial value 1 while the states 2–5 "rise" and "fall" in a sequence.

[1] A. S. Spirin, *Ribosomes* (Springer, New York, 2000).
[2] A. S. Spirin, FEBS Lett. **514**, 2 (2002).
[3] K. Abel and F. Jurnak, Structure (London) **4**, 229 (1996).
[4] J. Frank and C. M. T. Spahn, Rep. Prog. Phys. **69**, 1383 (2006).
[5] B. Alberts *et al.*, *Essential Cell Biology* (Garland Science, New York, 2003).
[6] J. D. Wen, L. Lancaster, C. Hodges, A. C. Zeri, S. H. Yoshimura, H. F. Noller, C. Bustamante, and I. Tinoco, Jr., Nature (London) **452**, 598 (2008).
[7] S. Redner, *A Guide to First-Passage Processes* (Cambridge University Press, New York, 2001).
[8] Y. R. Chemla, J. R. Moffitt, and C. Bustamante, J. Phys. Chem. B **112**, 6025 (2008).
[9] J. W. Shaevitz, S. M. Block, and M. J. Schnitzer, Biophys. J. **89**, 2277 (2005).
[10] J. C. Liao, J. A. Spudich, D. Parker, and S. L. Delp, Proc. Natl. Acad. Sci. U.S.A. **104**, 3171 (2007).
[11] M. Linden and M. Wallin, Biophys. J. **92**, 3804 (2007).
[12] M. Dixon and E. C. Webb, *Enzymes* (Academic Press, New York, 1979).
[13] M. E. Fisher and A. B. Kolomeisky, Proc. Natl. Acad. Sci. U.S.A. **96**, 6597 (1999).
[14] M. E. Fisher and A. B. Kolomeisky, Annu. Rev. Phys. Chem. **58**, 675 (2007).
[15] R. A. Marshall, C. E. Aitken, M. Dorywalska, and J. D. Puglisi, Annu. Rev. Biochem. **77**, 177 (2008).
[16] S. C. Blanchard, Curr. Opin. Struct. Biol. **19**, 103 (2009).
[17] S. Blanchard, R. L. Gonzalez, Jr., H. D. Kim, S. Chu, and J. D. Puglisi, Nat. Struct. Mol. Biol. **11**, 1008 (2004).
[18] S. Uemura, M. Dorywalska, T. H. Lee, H. D. Kim, J. D. Puglisi, and S. Chu, Nature (London) **446**, 454 (2007).
[19] J. B. Munro, A. Vaiana, K. Y. Sanbonmatsu, and S. C. Blanchard, Biopolymers **89**, 565 (2008).
[20] F. Vanzi, S. Vladimirov, C. R. Knudsen, Y. E. Goldman, and B. S. Cooperman, RNA **9**, 1174 (2003).
[21] Y. Wang, H. Qin, R. D. Kudaravalli, S. V. Kirillov, G. T. Dempsey, D. Pan, B. S. Cooperman, and Y. E. Goldman, Biochemistry **46**, 10767 (2007).
[22] D. Chowdhury, A. Schadschneider, and K. Nishinari, Phys. Life Rev. **2**, 318 (2005).
[23] C. MacDonald, J. Gibbs, and A. Pipkin, Biopolymers **6**, 1 (1968).
[24] C. MacDonald and J. Gibbs, Biopolymers **7**, 707 (1969).
[25] G. Lakatos and T. Chou, J. Phys. A **36**, 2027 (2003).
[26] L. B. Shaw, R. K. P. Zia, and K. H. Lee, Phys. Rev. E **68**, 021910 (2003).
[27] L. B. Shaw, J. P. Sethna, and K. H. Lee, Phys. Rev. E **70**,

021901 (2004).
[28] L. B. Shaw, A. B. Kolomeisky, and K. H. Lee, J. Phys. A **37**, 2105 (2004).
[29] T. Chou, Biophys. J. **85**, 755 (2003).
[30] T. Chou and G. Lakatos, Phys. Rev. Lett. **93**, 198101 (2004).
[31] J. J. Dong, B. Schmittmann, and R. K. P. Zia, J. Stat. Phys. **128**, 21 (2007).
[32] J. J. Dong, B. Schmittmann, and R. K. P. Zia, Phys. Rev. E **76**, 051113 (2007).
[33] B. Schmittmann and R. K. P. Zia, in *Phase Transition and Critical Phenomena*, edited by C. Domb and J. L. Lebowitz (Academic Press, New York, 1995), Vol. 17.
[34] G. M. Schütz, *Phase Transitions and Critical Phenomena* (Academic Press, New York, 2001), Vol. 19.
[35] A. Basu and D. Chowdhury, Am. J. Phys. **75**, 931 (2007).
[36] A. Basu and D. Chowdhury, Phys. Rev. E **75**, 021902 (2007).
[37] R. Phillips and S. R. Quake, Phys. Today **59** (5), 38 (2006).
[38] A. Garai, D. Chowdhury, and T. V. Ramakrishnan, Phys. Rev. E **79**, 011916 (2009).
[39] A. Garai, Ph.D. thesis, IIT Kanpur, 2009.
[40] H. Qian and E. L. Elson, Biophys. Chem. **101-102**, 565 (2002).
[41] B. P. English, W. Min, A. M. van Oijen, K. T. Lee, G. Luo, H. Sun, B. J. Cherayil, S. C. Kou, and X. S. Xie, Nat. Chem. Biol. **2**, 87 (2006).
[42] S. C. Kou, B. J. Cherayil, W. Min, B. P. English, and X. S. Xie, J. Phys. Chem. B **109**, 19068 (2005).
[43] W. Min, B. P. English, G. Luo, B. J. Cherayil, S. C. Kou, and X. S. Xie, Acc. Chem. Res. **38**, 923 (2005).
[44] W. Min, I. V. Gopich, B. P. English, S. C. Kou, X. S. Xie, and A. Szabo, J. Phys. Chem. B **110**, 20093 (2006).
[45] M. Basu and P. K. Mohanty, e-print arXiv:0901.2844.
[46] D. Keller and C. Bustamante, Biophys. J. **78**, 541 (2000).
[47] J. H. Jackson, T. M. Schmidt, and P. A. Herring, BMC Syst. Biol. **2**, 62 (2008).
[48] B. Derrida, J. Stat. Phys. **31**, 433 (1983).
[49] D. Sinha, U. Bhalla, and G. V. Shivashankar, Appl. Phys. Lett. **85**, 4789 (2004).
[50] M. E. Fisher and A. B. Kolomeisky, Physica A **274**, 241 (1999).
[51] N. G. Van Kampen, *Stochastic Processes in Physics and Chemistry* (Elsevier, New York, 1981).
[52] G. Hirokawa, N. Demeshkina, N. Iwakura, H. Kaji, and A. Kaji, Trends Biochem. Sci. **31**, 143 (2006).
[53] S. Petry, A. Weixlbaumer, and V. Ramakrishnan, Curr. Opin. Struct. Biol. **18**, 70 (2008).
[54] J. Krug, Phys. Rev. Lett. **67**, 1882 (1991).
[55] V. Popkov and G. Schütz, Europhys. Lett. **48**, 257 (1999).
[56] J. S. Hager, J. Krug, V. Popkov, and G. M. Schütz, Phys. Rev. E **63**, 056110 (2001).
[57] J. S. Hager, Phys. Rev. E **63**, 067103 (2001).
[58] T. Antal and G. M. Schütz, Phys. Rev. E **62**, 83 (2000).
[59] S. F. Tolić-Nørrelykke, A. M. Engh, R. Landick, and J. Gelles, J. Biol. Chem. **279**, 3292 (2003).